



Magnetic Supramolecular Nanofibers of Gold Nanorods for Photothermal Therapy

Qilin Yu, Ying-Ming Zhang, Yao-Hua Liu, and Yu Liu*

Molecular aggregation triggered by physical and chemical stimuli and based on multiple noncovalent interactions has immense potential utility for modeling and mimicking biological systems and for the diagnosis and treatment of degenerative diseases. Herein the preparation, properties, and biological activities of a new type of organic–inorganic hybrid supramolecular nanofiber composed of gold nanorods, mitochondrion-targeting-peptide-coated iron oxide nanoparticles, and hyaluronic-acid (HA)-modified β -cyclodextrin is reported. These photothermal nanofibers, which grew along the direction of the geomagnetic field, induced severe mitochondrial damage in human adenocarcinoma cells (A549); and, more strikingly, the nanofibers greatly suppress metastasis and clear A549 cells in tumor-bearing mice upon irradiation with a near-infrared laser. The ability to recruit HA-receptor-expressing tumor cells and to target mitochondria, as well as the high photothermal conversion efficiency imparted by the gold nanorods, makes these supramolecular nanofibers a promising nanotherapy for cancer in general and metastasis-related malignancy in particular.

Although medical therapies for treatment of well-confined primary tumors during early-stage cancer have advanced considerably,^[1] tumor invasion and metastasis remain intractable problems in cancer treatment. Metastasis is estimated to be responsible for most cancer-associated mortality because of the lack of surgical options and therapeutic agents for metastatic tumor cells.^[2] In fact, anticancer pharmacotherapies and surgeries frequently exacerbate tumor metastasis and hence increase the incidence of cancer-related death.^[3] Therefore, the development

of novel therapeutic strategies to suppress tumor growth and metastasis is imperative.

Recent breakthroughs involving supramolecular nanoassemblies, especially those derived from macrocyclic receptors, have had a strong impact on precision medicine.^[4] Tremendous effort has been devoted to exploring macrocycle-based nanomaterials with therapeutic potential.^[5] Particularly impressive progress has been achieved in the area of biocompatible nanomaterials that are responsive to multiple stimuli. Such materials are inherently flexible, dynamic, and adaptive to various internal and external stimuli and have been exploited for medical purposes.^[6] However, only a tiny fraction of the supramolecular nanoassemblies reported to date have a realistic chance of success in clinical trials, and expediting the development of multistimuli-responsive nanoassemblies with new modes of

action against life-threatening diseases, such as cancers, remains a challenge.

As part of our ongoing work on bioactive supramolecular assemblies,^[7] we herein report the construction of novel supramolecular nanofibers composed of noncovalently associated hyaluronic-acid-modified β -cyclodextrin (HACD) and mitochondrion-targeting-peptide-tethered inorganic gold nanorods (modified by lipoic acid (LA)) (AuNR-LA) and magnetic nanoparticles (MitP-MNPs) (Figure 1). Interestingly, the growth of the AuNR-MitP-MNP-HACD nanofibers was precisely regulated by the weak geomagnetic field, and the fibers could suppress tumor-cell metastasis by restricting the cells to a confined environment. In addition, bioactivity tests revealed that the photothermal AuNR-MitP-MNP-HACD supramolecular assemblies not only severely damaged mitochondria in human adenocarcinoma cells (A549) but also strongly inhibited disease progression in tumor-bearing mice upon irradiation with near-infrared (NIR) light, which is commonly used in photothermal therapy.^[8] Our results suggest that these unique organic–inorganic hybrid nanofibers may offer a promising strategy for suppressing tumor invasion and metastasis.

Multifunctional AuNR-MitP-MNP nanoconjugates were synthesized by combining MNPs and photothermal AuNRs (Figure 2a). First, Fe₃O₄ MNPs, which were synthesized by coprecipitation method,^[9] were silanized with aminopropyltriethoxysilane to afford MNPs-NH₂, which have chemically modifiable –NH₂ groups on the surface. Then a glutaraldehyde

Dr. Q. Yu, Dr. Y.-M. Zhang, Dr. Y.-H. Liu, Prof. Y. Liu
College of Chemistry, State Key Laboratory of Elemento-Organic
Chemistry
Nankai University
Tianjin 300071, P. R. China
E-mail: yuliu@nankai.edu.cn

Dr. Q. Yu
Key Laboratory of Molecular Microbiology and Technology
Ministry of Education, College of Life Sciences
Nankai University
Tianjin 300071, P. R. China

Prof. Y. Liu
Collaborative Innovation Center of Chemical Science and Engineering
Tianjin 300072, P. R. China

The ORCID identification number(s) for the author(s) of this article can be found under <https://doi.org/10.1002/adtp.201800137>

DOI: 10.1002/adtp.201800137

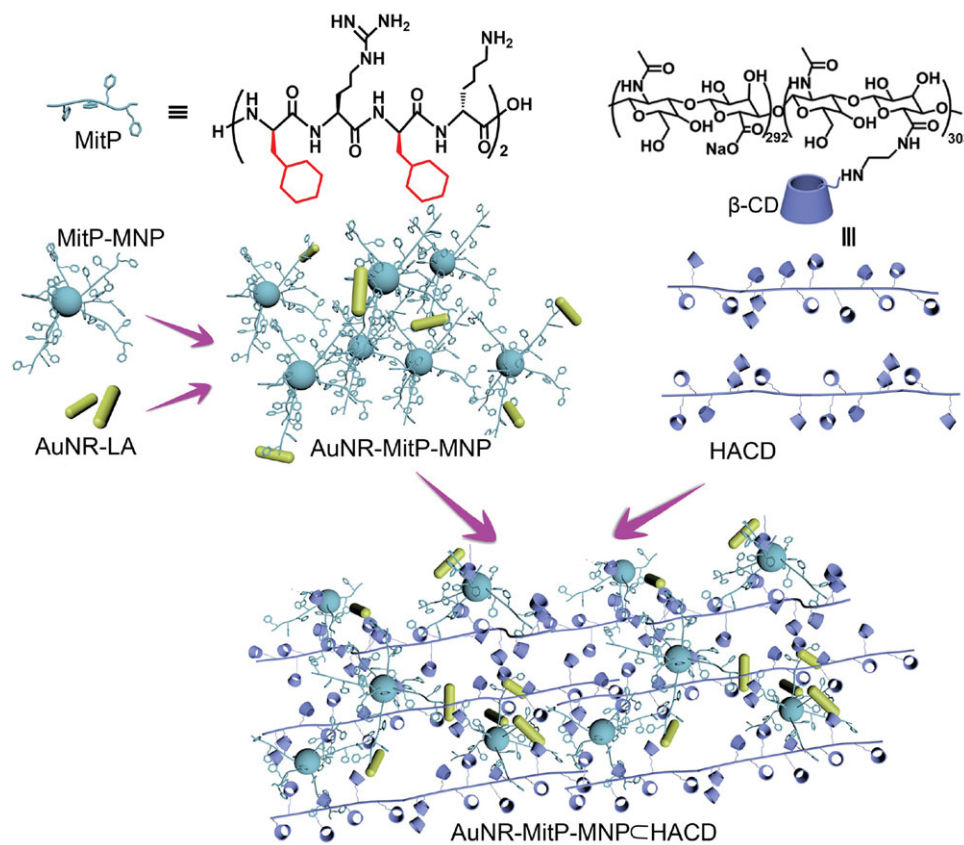


Figure 1. Schematic illustration of two-stage assembly of AuNR-MitP-MNP⊂HACD nanofibers.

linkage was used to decorate the MNPs-NH₂ with MitP, endowing the resulting MitP-MNPs with mitochondrion-specific targeting ability (Figure S1, Supporting Information). Second, a seed-mediated growth method was used to synthesize AuNRs,^[10] which had aspect ratios of 2–2.5. Decoration of the AuNRs with LA afforded AuNR-LA, which have –COOH groups on the surface. Finally, the MitP-MNPs and AuNR-LA were then conjugated by means of 1-ethyl-3-[3-dimethylaminopropyl]carbodiimide/*N*-hydroxysulfosuccinimide chemistry to obtain AuNR-decorated MNPs, designated AuNR-MitP-MNPs.

Owing to the presence of numerous pendant cyclohexylalanine groups on the surface of the AuNR-MitP-MNP nanoconjugates, they could be used to generate supramolecular nanoassemblies with hierarchical intermolecular organization. Specifically, reaction of HACD, a cross-linker containing abundant β-CD cavities,^[11] with the AuNR-MitP-MNPs formed AuNR-MitP-MNP⊂HACD supramolecular assemblies via multivalent binding between the β-CD cavities and the hydrophobic cyclohexyl groups of the MitP. TEM observation revealed that the AuNR-MitP-MNP⊂HACD assemblies were nanofibers with diameters of 100–500 nm and lengths of several micrometers, and that the AuNRs were randomly clustered on the surface of the fibers (Figure 2b). Elemental analysis by means of energy dispersive X-ray spectrometry (EDS) revealed the presence of Fe, Au, N, and O in the nanofibers (Figure 2c and Figure S2, Supporting Information). Inductively coupled mass spectrometry indicated

that the Fe/Au atomic ratio was ≈12 (Table S1, Supporting Information).

When separate aqueous suspensions of the AuNR-MitP-MNPs and the AuNR-MitP-MNP⊂HACD nanofibers were irradiated at 780 nm, the temperature of the suspensions increased rapidly and then stabilized, whereas no obvious temperature increase was observed upon irradiation of water alone (Figure 2d,e). These results indicate that both the nanoconjugates and the nanofibers had high photothermal conversion efficiencies.

Formation of the AuNR-MitP-MNP⊂HACD nanofibers was monitored in real time by light microscopy. When AuNR-MitP-MNPs and HACD were mixed together under the influence of the normal geomagnetic field (≈0.050 mT), they immediately interacted with each other, and within 2 min, they formed small aggregates (length 10–20 μm, Figure 3a–c). As the incubation time increased, the aggregates grew into short nanofibers (reaching 20–50 μm after 5 min) and eventually assembled into long higher-order nanofibers (50–200 μm after 10 min). Interestingly, the nanofibers self-assembled strictly along the direction of the geomagnetic field. When the orientation of the microscope relative to the geomagnetic field lines was changed, the growth direction of the nanofibers changed accordingly (Figure S3, Supporting Information). In contrast, when AuNR-MitP-MNPs and HACD were mixed together in a metal-caged room that was largely shielded from the geomagnetic field, the directional assemblies did not form (Figure 3d). Moreover, addition of

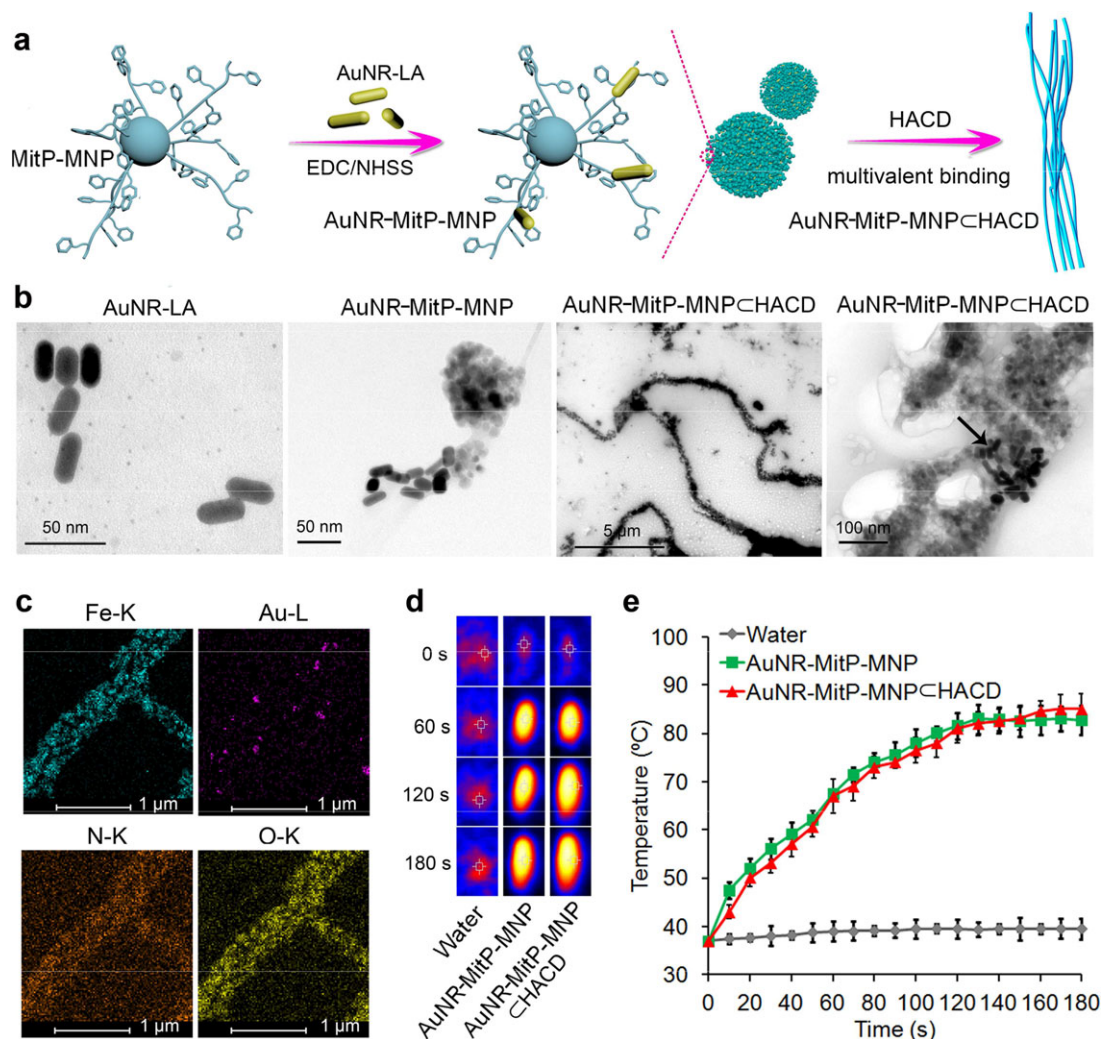


Figure 2. Preparation and characterization of photothermal supramolecular assemblies. a) Schematic illustration of AuNR-MitP-MNP \subset HACD nanofiber preparation. b) TEM images of AuNRs, AuNR-MitP-MNPs, and AuNR-MitP-MNP \subset HACD nanofibers. The black arrow indicates AuNRs on the nanofiber surface. c) EDS mapping images of AuNR-MitP-MNP \subset HACD nanofibers. d) Images of AuNR-MitP-MNPs and AuNR-MitP-MNP \subset HACD nanofibers under NIR laser irradiation (780 nm, 1 W, 20 W cm⁻²), recorded with an infrared camera. e) Temporal dependence of temperature during laser irradiation (780 nm, 1 W, 20 W cm⁻²) of aqueous AuNR-MitP-MNPs and AuNR-MitP-MNP \subset HACD nanofibers. There is no significant difference in temperature between the AuNR-MitP-MNP group and the AuNR-MitP-MNP \subset HACD group ($p < 0.05$).

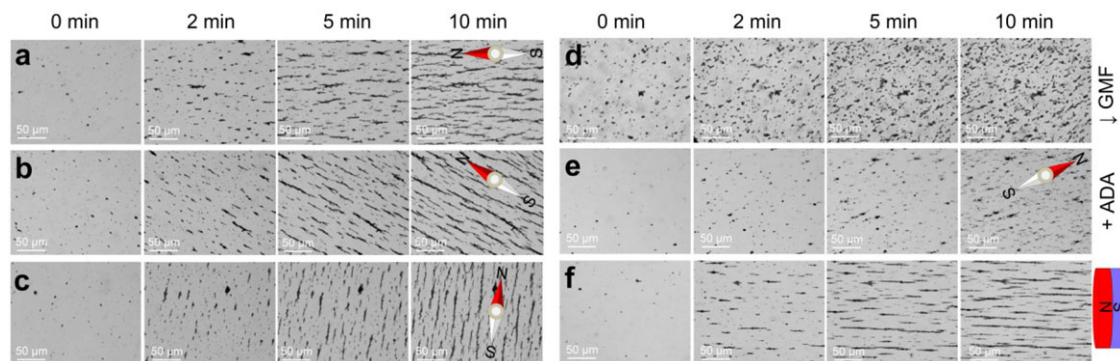


Figure 3. Light microscopy images showing magnetism-controlled assembly of AuNR-MitP-MNP \subset HACD nanofibers. a–c) Growth of AuNR-MitP-MNP \subset HACD nanofibers along the direction of the geomagnetic field (GMF, \approx 0.050 mT). d) Disruption of the directed assembly of AuNR-MitP-MNPs and HACD in a metal-caged room (GMF \approx 0.015 mT). e) Disruption of the directed assembly of AuNR-MitP-MNPs and HACD by addition of 1-adamantane carboxylic acid (ADA). f) Growth of AuNR-MitP-MNP \subset HACD nanofibers along the direction of an artificial magnetic field (\approx 0.160 mT).

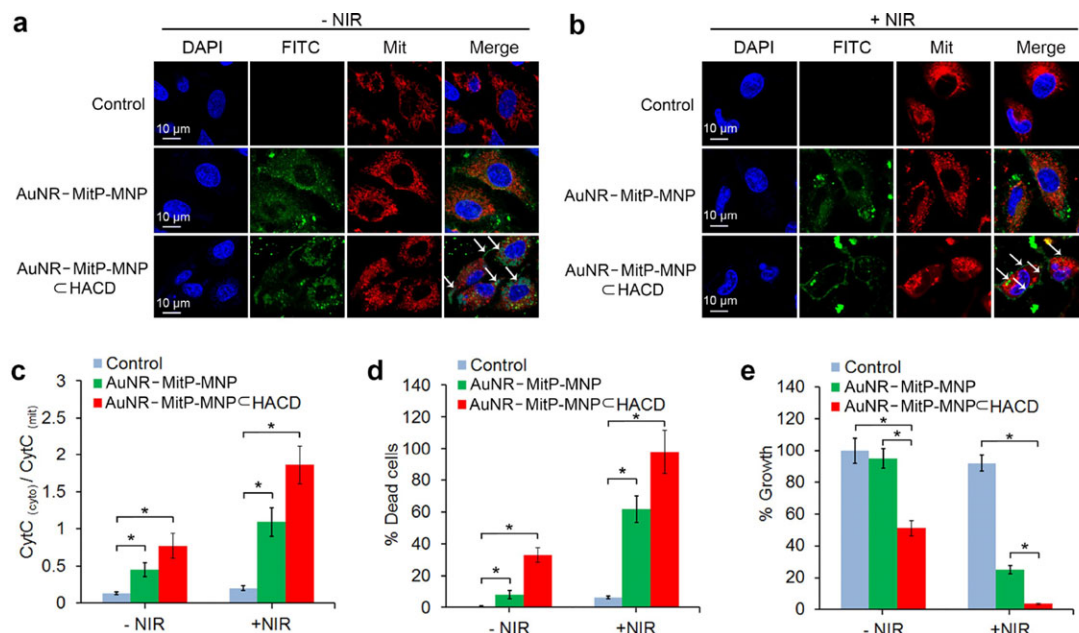


Figure 4. Effects of AuNR-MitP-MNP⊂HACD nanofibers on mitochondria and tumor cells. a) Confocal images of A549 cells treated with AuNR-MitP-MNPs (80 mg L^{-1}) or AuNR-MitP-MNP⊂HACD nanofibers (80 mg L^{-1} AuNR-MitP-MNPs plus 80 mg L^{-1} HACD). White arrows indicate nanofibers near or on mitochondria. b) Confocal microscopy images of treated cells after NIR irradiation (780 nm , 1 W , 20 W cm^{-2}) for 5 min. White arrows indicate nanofibers near or on mitochondria. c) Ratio of Cyt C_(cyto) to Cyt C_(mit), indicating that treatment with the AuNR-MitP-MNP⊂HACD nanofibers resulted in Cyt C release from the mitochondria to the cytosol. d) Cell death rate revealed by propidium iodide staining. e) Tumor cell growth rate revealed by CCK-8 assay. In panels (c)–(e), asterisks indicate statistically significant differences between groups ($p < 0.05$); error bars indicate standard deviations.

1-adamantane carboxylic acid (ADA) inhibited the directional assembling process (Figure 3e). These results confirmed that self-assembly of the AuNR-MitP-MNP⊂HACD nanofibers was induced by the geomagnetic field and was dependent on cyclodextrin-mediated supramolecular interaction.

Moreover, when a mixture of AuNR-MitP-MNPs and HACD was exposed to an artificial magnetic field ($\approx 0.160 \text{ mT}$), nanofibers immediately began to form and quickly grew along the direction of the magnetic field. Stable fibers were observed within 2–5 min (Figure 3f), and the growth of the nanofibers was accelerated when the magnetic field strength was increased (Table S2, Supporting Information).

Owing to the presence of MitP on the surface of the AuNR-MitP-MNP⊂HACD nanofibers, we hypothesized that they might be targetable to intracellular mitochondria. Indeed, we found that in the absence of NIR irradiation, both the AuNR-MitP-MNPs and the AuNR-MitP-MNP⊂HACD nanofibers co-localized preferentially with mitochondria in tumor cells (A549) and that the latter formed near or on the mitochondria (indicated by the white arrows in Figure 4a,b). Although both control cells and AuNR-MitP-MNP-treated cells had normal network-like mitochondria, the AuNR-MitP-MNP⊂HACD-treated cells displayed disrupted mitochondrial morphology, indicative of mitochondrial disruption. Moreover, when the treated cells were exposed to NIR irradiation, the presence of AuNR-MitP-MNPs had only a slight impact on the mitochondrial network; whereas irradiation in the presence of the AuNR-MitP-MNP⊂HACD nanofibers severely disrupted the mitochondria, leading to partial aggregation of the mitochondria or complete disappearance of this organelle (Figure 4b). Western blotting analysis of both Cyt C_(cyto) and Cyt

C_(mit) revealed that the presence of the AuNR-MitP-MNP⊂HACD nanofibers increased Cyt C release from the mitochondria to the cytosol, and this effect was augmented by NIR irradiation (Figure 4c).

Mitochondrial damage is known to induce cell death.^[12] Therefore, it is not surprising that compared with the AuNR-MitP-MNPs, the AuNR-MitP-MNP⊂HACD nanofibers caused the death of more tumor cells ($\approx 35\%$) and a greater decrease in cell growth ($\approx 50\%$), even in the absence of NIR irradiation (Figure 4d,e). In addition, NIR irradiation enhanced the toxicity of the nanofibers. Under NIR irradiation, treatment with the AuNR-MitP-MNPs led to a cell death rate of $\approx 60\%$ and reduced cell growth by $\approx 25\%$, but treatment with the AuNR-MitP-MNP⊂HACD nanofibers caused almost 100% cell death and 100% growth inhibition (Figure 4d,e).

Tumor cell invasion and metastasis frequently contribute to cancer-associated mortality.^[13] Because HACD can strongly bind tumor cells,^[11,14] we hypothesized that the AuNR-MitP-MNP⊂HACD nanofibers might suppress tumor invasion and metastasis. To verify this hypothesis, we used a Matrigel invasion model to investigate the effects of the nanofibers on invasion of RFP-tagged A549 cells (Figure 5a). Confocal microscopy showed that the AuNR-MitP-MNPs were uniformly distributed in the Matrigel and had little impact on cell invasiveness (Figure 5b–d). In contrast, the AuNR-MitP-MNP⊂HACD nanofibers formed around the tumor cells in the Matrigel, which resulted in aggregation of the cells and severely attenuated their invasion into the gel (Figure 5b–d). Interestingly, nanofibers were not observed inside the invading cells, suggesting that the gel inhibited nanofiber internalization by the cells (Figure S4, Supporting

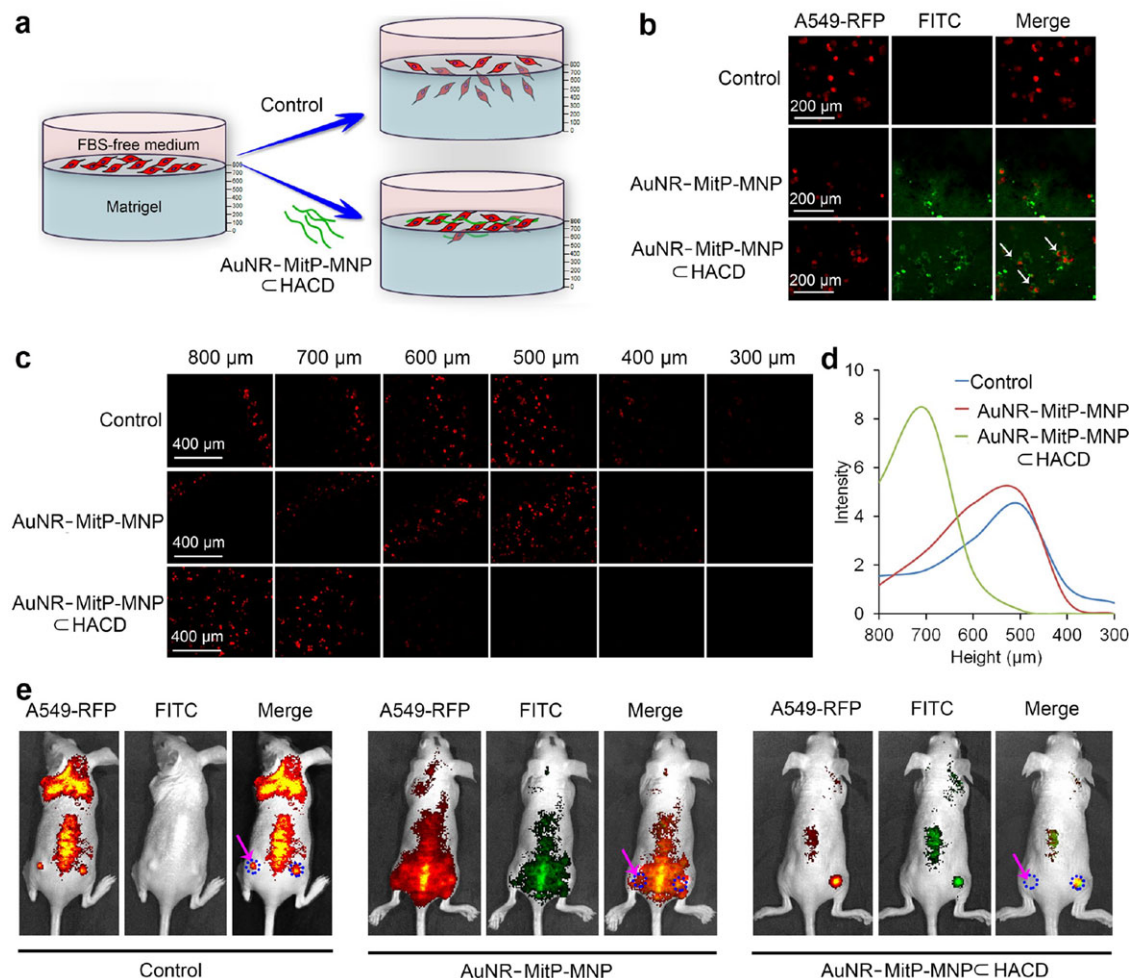


Figure 5. Effects of AuNR-MitP-MNP⊂HACD nanofibers on tumor-cell invasion, metastasis, and survival both in vitro and in vivo. a) Schematic illustration of suppression of tumor-cell invasion into Matrigel by AuNR-MitP-MNP⊂HACD nanofibers. Note that while AuNR-MitP-MNP has only a slight inhibitory on tumor-cell invasion (at the height of 400 μm), AuNR-MitP-MNP⊂HACD severely suppresses invasion (at 600 μm to 400 μm). b) Confocal microscopy images of invading cells treated with AuNR-MitP-MNPs or AuNR-MitP-MNP⊂HACD nanofibers. The white arrows indicate nanofibers around the RFP-tagged A549 cells. c) Confocal microscopy images of the invading tumor cells at various heights in the Matrigel. d) Quantification of fluorescence intensities of tumor cells at various heights in the Matrigel. e) In vivo suppression of A549-RFP cell metastasis and survival by AuNR-MitP-MNP⊂HACD nanofibers in combination with NIR laser irradiation. The dotted blue circles indicate tumor-cell injection sites; the purple arrows indicate the NIR laser irradiation site (780 nm, 1 W, 20 W cm⁻²). The FITC images show the distribution of FITC-tagged nanocomposites.

Information). These results indicate that the extracellular self-assembled nanofibers confined the tumor cells and hence suppressed their invasion into the gel.

Hyaluronic acid (HA) targets tumors by interacting with the HA receptor, which is overexpressed in tumor cells.^[11,14] We hypothesized that the AuNR-MitP-MNP⊂HACD nanofibers may specifically target the tumor cells in vivo. The effects of the AuNR-MitP-MNP⊂HACD nanofibers on tumor metastasis in vivo were investigated in a mouse model. Mice that had been inoculated with RFP-tagged tumor cells, were treated with AuNR-MitP-MNPs or AuNR-MitP-MNP⊂HACD nanofibers (Figure 5e). The former had only a slight impact on tumor metastasis; in this group, as in the control group, extensive migration of the tumor cells from the injection sites to the neck was observed. The poor anti-tumor activity of AuNR-MitP-MNPs may be attributed to its failure to confine the tumor cells at the injection sites, leading

to escape of the tumor cells from these sites. In striking contrast, the AuNR-MitP-MNP⊂HACD nanofibers were found almost exclusively in the region where tumor cells were located, and the nanofibers confined the tumor cells to the injection sites (Figure 5e), suggesting that the nanofibers effectively suppressed tumor-cell metastasis.

The photothermal properties of the AuNR-MitP-MNPs and the AuNR-MitP-MNP⊂HACD nanofibers were evaluated in vivo as well. Six hours after administration of the nanocomposites, the tumor-injection sites were irradiated by the NIR laser, and the local temperature was monitored in real time. Compared with the control group and the AuNR-MitP-MNP-treated group, the AuNR-MitP-MNP⊂HACD-treated group showed a dramatic increase in temperature (from ≈37 °C to ≈56 °C) after 180 s of irradiation (Figure S5, Supporting Information). On the third day after irradiation, tumor cells were completely

cleared from the irradiation site in the nanofiber-treated group, whereas live tumor cells were detected in the control group and the AuNR-MitP-MNP-treated group. Furthermore, accumulation of the nanofibers in the reticuloendothelial system organs (including the liver, spleen, and kidney) was minimal and had no impact on the histological structures of these organs (Figure S6, Supporting Information), confirming that the nanofibers had good tumor-targeting specificity and good biocompatibility. In addition, no nanofibers were detected at the irradiation site (Figure 5e), indicating that they migrated away from the irradiation site after clearance of the tumor cells. Taken together, these results suggest that the biocompatible photothermal supramolecular nanofibers could efficiently suppress tumor-cell metastasis and kill tumor cells when used in combination with NIR irradiation.

In conclusion, novel geomagnetism-responsive photothermal supramolecular nanofibers composed of AuNR-conjugated MitP-bearing MNPs and HA-modified β -CD were fabricated for treatment of tumor cells via photothermal activation. The combination of the magnetic core and the MitP promoted the internalization of the nanofibers in cancer cells and imparted specificity for mitochondria. In addition, the noncovalent bound HACD not only endowed the nanofibers with the desired ability to specifically recognize HA-receptor-expressing cancer cells but also facilitated the spontaneous formation of geomagnetism-sensitive nanofibers that actively restricted malignant cells to a confined environment, especially around the location of primary tumors. As a result of the photothermal properties originating from the AuNRs in the AuNR-MitP-MNP/HACD nanofibers, NIR irradiation induced severe mitochondrial damage, caused cell death *in vitro*, and suppressed tumor-cell invasion and metastasis *in vivo*. Given the attractive structural and functional features of the AuNR-MitP-MNP/HACD nanofibers, we anticipate that future research on these and other stimuli-responsive supramolecular assemblies will facilitate the development of next-generation cancer therapies.

Experimental Section

Chemicals and Materials: Aminopropyltriethoxysilane, HAuCl₄, cetyltrimethyl ammonium bromide, and glutaraldehyde were purchased from Sigma (USA). All other reagents were purchased from Aladdin (China). HACD was synthesized by means of an amide condensation reaction between hyaluronic acid sodium salt and mono-6-deoxyl-6-ethylenediamino- β -CD, according to a previously reported procedure.^[11]

Instrumentation: The morphologies of the AuNRs, the AuNR-MitP-MNPs, and the AuNR-MitP-MNP/HACD nanofibers were characterized by transmission electron microscopy (TEM; JEM 1200EX, Kaisha, Japan). Energy-dispersive X-ray spectroscopy (EDS) mapping images were acquired by high-resolution TEM (Tecnai G2 F20 S-TWIN, FEI, USA). The crystal structure and composition of the MNPs were characterized by X-ray diffraction analysis (D/max-2500, Japan). The amounts of Fe and Au in AuNR-MitP-MNP/HACD were determined by inductively coupled plasma optical emission spectrometry (Optima 8300, PerkinElmer, USA). *In vivo* distributions of tumor cells, AuNR-MitP-MNPs, and AuNR-MitP-MNP/HACD were monitored with a multispectral small-animal imaging system (IVIS Lumina II, Xenogen, USA). Geomagnetic field strength was measured with a standard Gauss meter (Beiyi-601, Pafei, China). Supramolecular nanoassemblies and cells were observed with a light microscope (CKX53, Olympus, Japan) and a confocal microscope (FV1000, Olympus, Japan). A NIR laser beam was produced with a NIR laser sys-

tem (780 nm, 1 W, 20 W cm⁻², Shuanghong, China). The photothermal properties of AuNR-MitP-MNPs and AuNR-MitP-MNP/HACD were monitored by an infrared thermal imaging camera (Xintest, China). Cell death was quantified with a flow cytometer (FACS Calibur, BD, USA).

Preparation of Photothermal Supramolecular Assemblies: Fe₃O₄ MNPs were prepared by a co-precipitation method.^[9] For preparation of MitP-MNPs, MNPs (40 mg) were suspended in 40 mL of ethanol, and then 2 mL of aminopropyltriethoxysilane was added. The mixture was magnetically stirred at 85 °C for 2 h and then centrifuged, and the pellet was washed three times with ethanol and twice with distilled water to afford MNPs-NH₂. The MNPs-NH₂ were suspended in 30 mL of 8% glutaraldehyde prepared in phosphate buffered saline (PBS, pH 7.4). The suspension was gently shaken for 6 h at room temperature and then centrifuged to pellet MNPs-NH₂-glutaraldehyde. The pellet was washed three times with PBS and then suspended in 20 mL of the same buffer. 400 μ L of MitP labeled with fluorescein isothiocyanate (FITC) (FITC-ACP-Fx-r-Fx-K-Fx-r-Fx-K, 1 mM in PBS) was added to the suspension, which was then shaken at 120 rpm at 4 °C for 24 h. The resulting solid was separated by centrifugation, and the pellet was washed twice with distilled water and lyophilized in a vacuum freeze dryer to afford MitP-MNPs.^[7]

AuNRs were synthesized according to El-Sayed's method.^[10] Then 10 mg of the obtained AuNRs was suspended in 10 mL of distilled water, and 1 mg of LA was added. The mixture was sonicated for 10 min (AS3120, 250 W, AutoScience, China) and centrifuged, and the pellet was washed with distilled water to afford AuNR-LA. AuNR-LA (10 mg) was mixed with 50 mg of the MitP-MNPs in 50 mM PBS (pH 7.2), and then 21 mg of 1-ethyl-3-[3-dimethylaminopropyl]carbodiimide and 22 mg of *N*-hydroxysulfosuccinimide were added. The solutions were sonicated for 2 h and centrifuged to obtain AuNR-MitP-MNPs.

The AuNR-MitP-MNP/HACD nanofibers were generated by mixing AuNR-MitP-MNPs and HACD (each at a concentration of 80 mg L⁻¹) and sonicating the mixture for 5 min.

Photothermal Analysis: To measure photothermal conversion efficiency, solutions of AuNR-MitP-MNPs (80 mg L⁻¹) or AuNR-MitP-MNP/HACD nanofibers (80 mg L⁻¹ AuNR-MitP-MNPs plus 80 mg L⁻¹ HACD) were irradiated with a NIR laser (780 nm, 1 W, 20 W cm⁻²) for 180 s. Temperature was monitored in real time with an infrared thermal imaging camera.

Confocal Microscopy: Human lung adenocarcinoma cells (A549, Cell Resource Center, China Academy of Medical Science, Beijing, China) were incubated with AuNR-MitP-MNPs (80 mg L⁻¹) or with AuNR-MitP-MNP/HACD nanofibers (80 mg L⁻¹ AuNR-MitP-MNPs plus 80 mg L⁻¹ HACD) for 24 h. The cells were then washed with PBS and stained with MitoTracker Red (100 nM, Sigma) at 37 °C for 40 min. The cells were further fixed with ice-cold methanol and stained with 4',6-diamidino-2-phenylindole (DAPI, 5 mg L⁻¹, Sigma), and then observed by confocal microscopy.

Cell Viability Assay: To evaluate the growth of the A549 cells, they were treated with AuNR-MitP-MNPs or AuNR-MitP-MNP/HACD nanofibers for 24 h as described in the preceding section. The extent of growth of the treated cells was then determined with a CCK-8 assay kit (Dojindo, Japan). After 24 h of treatment, cell death rate was assessed by means of propidium iodide staining and subsequent flow cytometry analysis.

Western Blotting: For detection of cytosolic and mitochondrial cytochrome C (Cyt C_(cyto) and Cyt C_(mit)), treated A549 cells were homogenized with a Dounce homogenizer (20–50 strokes). The cell lysate was centrifuged at 1000 \times g and 4 °C to remove nuclei and intact cells. The resulting suspension was then centrifuged at 10 000 \times g to obtain the cytosol (supernatant) and the mitochondria (pellet), respectively. The levels of Cyt C_(cyto) and Cyt C_(mit) were determined with Cyt C monoclonal antibody (Abcam, USA). The Cyt C_(cyto)/Cyt C_(mit) ratio was quantified by the Image J software (ver. 2, USA).

In Vitro Tumor-Cell Invasion Assay: A549 cells tagged with red fluorescent protein (RFP) (A549-Luc2-tdT-2, Cell Resource Center, China Academy of Medical Science, Beijing, China) were cultured in McCoy's 5A medium supplemented with 10% fetal bovine serum (Hyclone, Australia) in a CO₂ incubator at 37 °C for 48 h. The cells were then suspended in fetal-bovine-serum-free McCoy's 5A medium at 5 \times 10⁵ cells mL⁻¹. Matrigel (Corning, USA) was diluted in coating buffer (0.01 M Tris, 0.7% NaCl, pH 8.0) to a

final concentration of 300 $\mu\text{g mL}^{-1}$ and then placed in 24-well invasion chambers (immersed in McCoy's 5A medium supplemented with 10% fetal bovine serum) to a gel height of 800 μm . The chambers were incubated at 37 °C for 2 h for gelation. Cell suspension (500 μL) was added to the chambers, and then AuNR-MitP-MNPs (80 mg L^{-1}) or AuNR-MitP-MNP \square HACD nanofibers (80 mg L^{-1} AuNR-MitP-MNPs plus 80 mg L^{-1} HACD) were added. The cells were cultured for 12 h, and the invading cells were then observed by confocal microscopy. The fluorescence intensities of the cells at different heights in the Matrigel were quantified by the Image J software.^[7] For detection of intracellular formation of AuNR-MitP-MNP \square HACD nanofibers, the Matrigel was treated with trypsin (2.5%, Gibco, USA) and washed with PBS to release the invading cells. The released cells were washed three times with PBS and observed by fluorescence microscopy.

In Vivo Metastasis Assay: In vivo tumor metastasis was evaluated in A549-Luc2-tdT-2-bearing nude mice (Huaifukang, China) as follows. Fifteen 4-week-old female BALB/c nude mice were pretreated with cyclophosphamide (200 mg kg^{-1}) for 2 days. Then the mice were subcutaneously inoculated at two sites near the rear legs with 100 μL of A549-Luc2-tdT-2 cell suspension (1×10^8 cells mL^{-1}) and divided into two treatment groups and a control group (five mice per group). Three days after inoculation, AuNR-MitP-MNPs (80 mg kg^{-1}) or AuNR-MitP-MNP \square HACD nanofibers (80 mg kg^{-1} AuNR-MitP-MNPs plus 80 mg kg^{-1} HACD) were intravenously administered via the tail vein to the mice; a control group received only saline. Six hours after administration, one of the inoculation sites was irradiated by a NIR laser for 10 min. The distributions of the A549-Luc2-tdT-2 cells and the nanocomposites in the mice were observed 2 days after administration. All animal experiments were approved by the Animal Care and Use Committee at Nankai University.

Statistical Analysis: Three replicates of each experiment were performed, and values reported herein are means \pm standard deviations. Differences between groups were compared by a one-way analysis of variance test ($p < 0.05$). All statistical tests were performed using the SPSS software package (ver. 20, IBM, USA).

Supporting Information

Supporting Information is available from the Wiley Online Library or from the author.

Acknowledgements

This work was funded by the National Natural Science Foundation of China (grants 21432004, 31870139, 21472100, 21772099, and 91527301).

Conflict of Interest

The authors declare no conflict of interest.

Keywords

cyclodextrin, gold nanorods, photothermal therapy, supramolecular nanofibers, tumor metastasis

Received: October 24, 2018

Revised: November 17, 2018

Published online:

- [1] a) A. Becker, B. K. Thakur, J. M. Weiss, H. S. Kim, H. Peinado, D. Lyden, *Cancer Cell* **2016**, *30*, 836; b) C. Jiang, X. Li, H. Zhao, H. Liu, *Mol. Cancer* **2016**, *15*, 62.
- [2] a) T. Li, J. Xie, C. Shen, D. Cheng, Y. Shi, Z. Wu, H. Li, *Oncogene* **2016**, *35*, 1575; b) J. Massagué, A. C. Obenauf, *Nature* **2016**, *529*, 298.
- [3] a) M. Horowitz, E. Neeman, E. Sharon, S. Ben-Eliyahu, *Nat. Rev. Clin. Oncol.* **2015**, *12*, 213; b) G. S. Karagiannis, J. S. Condeelis, M. H. Oktay, *Clin. Exp. Metastasis* **2018**, *35*, 269; c) J. M. Ebos, *Cancer Res.* **2015**, *75*, 3427.
- [4] a) S. Mura, J. Nicolas, P. Couvreur, *Nat. Mater.* **2013**, *12*, 991; b) R. Dong, Y. Zhou, X. Huang, X. Zhu, Y. Lu, J. Shen, *Adv. Mater.* **2015**, *27*, 498; c) J. Boekhoven, S. I. Stupp, *Adv. Mater.* **2014**, *26*, 1642.
- [5] a) X. Yan, F. Wang, B. Zheng, F. Huang, *Chem. Soc. Rev.* **2012**, *41*, 6042; b) M. J. Webber, E. A. Appel, E. W. Meijer, R. Langer, *Nat. Mater.* **2016**, *15*, 13; c) H.-L. Sun, Y. Chen, X. Han, Y. Liu, *Angew. Chem.* **2017**, *129*, 7168; d) H. S. Choi, *Nat. Nanotechnol.* **2014**, *9*, 93.
- [6] a) Y. Chen, Y. Liu, *Adv. Mater.* **2015**, *27*, 5403; b) G. Yu, Z. Yang, X. Fu, B. C. Yung, J. Yang, Z. Mao, L. Shao, B. Hua, Y. Liu, F. Zhang, Q. Fan, S. Wang, O. Jacobson, A. Jin, C. Gao, X. Tang, F. Huang, X. Chen, *Nat. Commun.* **2018**, *9*, 766; c) A. Harada, Y. Takashima, M. Nakahata, *Acc. Chem. Res.* **2014**, *47*, 2128.
- [7] Q. Yu, Y. M. Zhang, Y. H. Liu, X. Xu, Y. Liu, *Sci. Adv.* **2018**, *4*, eaat2297.
- [8] a) B. Shi, Q. Yan, J. Tang, K. Xin, J. Zhang, Y. Zhu, G. Xu, R. Wang, J. Chen, W. Gao, T. Zhu, J. Shi, C. Fan, C. Zhao, H. Tian, *Nano Lett.* **2018**, *18*, 6411; b) Q. Li, Q. Wang, S. Wang, S. Zhu, T. Yuan, Z. Guo, J. Cao, H. Tian, W. H. Zhu, *Adv. Ther.* **2018**, *1*, 1800093; c) J. Wu, Y. Xu, D. Li, X. Ma, H. Tian, *Chem. Commun.* **2017**, *53*, 4577; d) Y. Hao, Y. Chen, M. Lei, T. Zhang, Y. Cao, J. Peng, L. Chen, Z. Qian, *Adv. Ther.* **2018**, *1*, 1800008; e) H. Y. Yang, Y. Li, D. S. Lee, *Adv. Ther.* **2018**, *1*, 1800011.
- [9] T. Ahn, J. H. Kim, H.-M. Yang, J. W. Lee, J. D. Kim, *J. Phys. Chem. C* **2012**, *116*, 6069.
- [10] B. Nikoobakht, M. A. El-Sayed, *Chem. Mater.* **2003**, *15*, 1957.
- [11] Y. Yang, Y.-M. Zhang, Y. Chen, J.-T. Chen, Y. Liu, *J. Med. Chem.* **2013**, *56*, 9725.
- [12] G. Kroemer, J. C. Reed, *Nat. Med.* **2000**, *6*, 513.
- [13] a) P. S. Steeg, *Nat. Med.* **2006**, *12*, 895; b) S. Valastyan, R. A. Weinberg, *Cell* **2011**, *147*, 275.
- [14] N. Li, Y. Chen, Y.-M. Zhang, Y. Yang, Y. Su, J.-T. Chen, Y. Liu, *Sci. Rep.* **2015**, *4*, 4164.